Hindawi
Journal of Spectroscopy
Volume 2018, Article ID 8573014, 12 pages
https://doi.org/10.1155/2018/8573014

Research Article

FT-IR, Laser-Raman, UV-Vis, and NMR Spectroscopic Studies of Antidiabetic Molecule Nateglinide

Tuba Özdemir Öge

Vocational School of Health Services, Bartın University, 74100 Bartın, Turkey

Correspondence should be addressed to Tuba Özdemir Öge; tozdemir@bartin.edu.tr

Received 5 June 2018; Accepted 26 August 2018; Published 24 September 2018

Academic Editor: Rizwan Hasan Khan

The quantum chemical calculations and spectroscopic and theoretical characterizations of nateglinide molecule, a derivative of meglitinide and an oral antidiabetic drug, were performed using FT-IR, Laser-Raman, and NMR chemical shift and UV-Vis analysis methods. The other parameters including geometric structures, optimized geometry, vibrational frequencies, dipole moments, infrared and Raman intensities, and HOMO and LUMO energies of nateglinide molecules were studied using the density functional theory. In addition, the ^{13}C and ^{1}H NMRs were calculated using Gaussian 09 program with the DFT/B3LYP method at the 6-31G + (d, p) basis set. TD-DFT calculations were performed to examine the electronic transitions including orbital energies, absorption wavelengths, oscillator strengths, and excitation energies in methanol. The research was performed to provide detailed spectroscopic information of antidiabetic nateglinide molecule's monomer conformations.

1. Introduction

Meglitinides (glitinides) are insulin secretagogues, and they stimulate insulin release from pancreas [1–3]. Nateglinide, a derivative of meglitinide, is an oral antidiabetic drug used for the treatment of type II diabetes mellitus. Nateglinide lowers the blood glucose levels by stimulating insulin secretion from the pancreas. The structure name of nateglinide is (−)-*N*-[(*trans*-4-isopropylcyclohexane) carbonyl]-D-phenylalanine [4–7]. The chemical formula of nateglinide used in the present study is $C_{19}H_{27}NO_3$. The CAS and MDL numbers are 105816-04-4 and MFCD00875706, respectively. The molecular weight of nateglinide is 317.42 g/mol. The synonyms of nateglinide are given as Fastic, *N*-[(*trans*-4-isopropylcyclohexyl)carbonyl]-D-phenylalanine, Starlix, and Starsis in [8].

Jain et al. carried out a work on spectrophotometric determination of nateglinide in bulk and tablet dosage forms [9]. Babu et al. investigated nateglinide with visible spectrophotometry and spectrophotometric methods [10, 11]. Bruni et al. developed a method for the quantification of the polymorphic purity of nateglinide in mixtures formed by polymorphs H and B [12]. Guardado-Mendoza et al. explained that nateglinide and repaglinide are effective in reducing postprandial glucose excursion and HbA1c levels from 0.8% to 1% in T2DM [13]. Rani et al. described two spectrophotometric methods for the determination of nateglinide [14]. Goyal et al. determined the crystal structure and crystallographic parameters of experimentally crystallized polymorphs of nateglinide. Crystallographic parameters of nateglinide polymorphs were given as Form H, Form B, Form MS, and Form S (space groups are P-1, C2, P-4, and P-42C), and the forms were found to exist in triclinic, monoclinic, tetragonal, and tetragonal, correspondingly [15]. Remko [16] used the methods of theoretical chemistry to elucidate the molecular properties of the hypoglycemic sulfonylureas and glinides (acetohexamide, tolazamide, tolbutamide, chlorpropamide, gliclazide, glimepiride, glipizide, glibenclamide, nateglinide, and repaglinide) which are known as antidiabetic molecules. The geometry and energy of these drugs were computed using the Becke3LYP/6-31G + (d, p) method. Karakaya et al. [17] investigated the vibrational and structural properties of tolazamide molecule. Ozdemir and Gokce studied the glimepiride molecule as a sulfonylurea compound using FT-IR, Raman and NMR spectroscopy, and DFT theory [18].

Few studies have been encountered on investigation of nateglinide molecule, which is effectively used against diabetes mellitus. In this regard, the present research was carried out to perform a detailed theoretical and experimental investigation of nateglinide, which is the active ingredient of an antidiabetic drug commonly prescribed as Starlix, using spectroscopic analyses such as FT-IR, Laser-Raman, UV-Vis, and NMR. In the present study, density functional theory study was theoretically performed to obtain the vibrational wavenumbers, FT-IR, Laser-Raman, and NMR chemical shifts and UV-Vis of nateglinide molecule. The recorded experimental data were supported with the computed parameters using theoretical methods at DFT/B3LYP/6-31G + (d, p) level. The obtained theoretical and experimental results were used to give detailed information of the molecular electronic structure of nateglinide.

2. Experimental and Computational Procedures

Nateglinide was purchased from Sigma-Aldrich Corporation in powder form. The melting point of nateglinide is in the range of 137°C–141°C. The chemical name of nateglinide (NTG) is *N*-(*trans*-4-isopropylcyclohexyl carbonyl)-D-phenylalanine. This molecule is almost insoluble in water, and highly soluble in methylene and methanol chloride. It shows polymorphism [19]. The optimized monomer structures of antidiabetic molecule are given in Figure 1. The FT-IR spectrum of nateglinide molecule was recorded within 400–4000 cm^{-1} region at room temperature, using the potassium bromide (KBr) pellet, on a Fourier-transform infrared spectrometer in the solid phase of the sample as shown in Figure 2. The Laser-Raman spectrum was recorded at room temperature in 100–4000 cm^{-1} region as shown in Figure 3. The ^{1}H and ^{13}C NMR chemical shift spectra of the compound solved in dimethyl sulfoxide (DMSO-d6) were recorded with TMS as the internal standard using the Premium Compact NMR device at 600 MHz frequency and 14.1 Tesla field power. The chemical shifts were reported at ppm level as given in Figures 4 and 5. The ultraviolet visible spectrum of nateglinide dissolved in methanol was recorded using a UV-Vis spectrophotometer in 200–400 nm range at room temperature as given in Figure 6.

B3LYP (Becke, three-parameter, Lee–Yang–Parr) level with 6-31G + (d, p) basis set was used to compute the electronic structure properties of nateglinide molecule [20, 21]. Vibrational wavenumbers, geometric parameters, and molecular properties were calculated using Gaussian 09W software and GaussView5 molecular visualization program on a computer system [22–24]. Veda 4 program was used to compute the potential energy distribution of vibrational wavenumbers as given in Table 1 [25]. The major contributions for the computed electronic wavelengths were obtained by GaussSum 3.0 program as listed in Table 2 [26].

3. Results and Discussion

3.1. Geometric Structure. The experimental data explain the crystallographic structure of nateglinide [27], and these findings were compared with the calculated results as given in Table 3. The other geometric parameters such as bond lengths, bond angles, and torsion angles with the corresponding literature information are given in Table 3. Zero-point, relative energy values, and dipole moments are given in Table 4. Tessler and Goldberg investigated bis(nateglinide) hydronium chloride, in addition to its self-assembly into extended polymeric arrays with O-H···O, N-H···Cl, and O-H···Cl hydrogen bonds. The title compound contains four dissimilar moieties which are conformationally different in the asymmetric unit [27].

The C-C bond lengths of the title molecule were calculated at the interval of 1.395–1.558 Å, while they were recorded between 1.352 and 1.543 Å in the literature [27]. The C-N bond lengths of the title molecule were calculated at 1.447 Å and 1.372 Å, while they were recorded at 1.460 Å and 1.332 in the literature [27]. In this research, the C-H bond lengths of the title molecule were calculated at the interval of 1.086–1.103 Å. The calculated C11-C13, C13-C15, C9-C11, C7-C9, C7-C17, C15-C17, C17-C18, C18-C21, C21-C23, C24-C25, C25-C38, C35-C38, C33-C35, C33-C30, C27-C30, C25-C27, C33-C41, C41-C47, and C41-C43 bond lengths for nateglinide are 1.398 Å, 1.395 Å, 1.396 Å, 1.398 Å, 1.401 Å, 1.403 Å, 1.514 Å, 1.558 Å, 1.525 Å, 1.530 Å, 1.546 Å, 1.537 Å, 1.542 Å, 1.542 Å, 1.539 Å, 1.539 Å, 1.554 Å, 1.539 Å, and 1.539 Å, respectively. The calculated bond angles of C24-C25-C27, C24-C25-C38, C25-C27-C30, C25-C38-C35, C38-C35-C33, C35-C33-C30, and C33-C30-C27 are 117.171°, 109.582°, 110.933°, 111.408°, 112.186°, 109.752°, and 112.163°, respectively, in this study. The calculated dihedral angle of C9-C7-C17-C18 is −179.489°.

Jain et al. studied the monomers, dimers, and tetramers of nateglinide to understand the conformational properties. Nateglinide molecule contains two strong hydrogen bond donors as N–H/O–H and two strong acceptors as 2 × C = O [28]. As in the present research, two conformations come into prominence, namely, N-A and N-C. These two differ from others by the relative position of hydrogen in the carboxylic group and by torsional angle across C2–C3–N4–C5 (−169.17° in N-A and −118.57° in N-C). Likewise, the torsional angles of Monomer 1 and Monomer 2 were calculated −169.15007° and −120.87747°, respectively, in the present research.

3.2. Vibrational Frequency Analyses. In the following discussion, nateglinide is experimentally examined using FT-IR, Laser-Raman, UV-Vis spectroscopy, and NMR. The observed and calculated vibrational frequencies, observed and calculated FT-IR intensities, Raman scattering activities, and vibrational assignments of the title molecule are given in Table 1. Nateglinide consists of 50 atoms, and accordingly, it has 144 modes of vibrations according to the relation 3N-6 (for $N = 50$). In the present research, C-H, C-O, O-H, N-H, and C-C vibrations were examined. As shown in Figures 2 and 3 and Table 1, the experimental and calculated vibrational wavenumbers are in good agreement.

The computations of harmonic wavenumbers, IR intensities, and Raman activities were performed with the

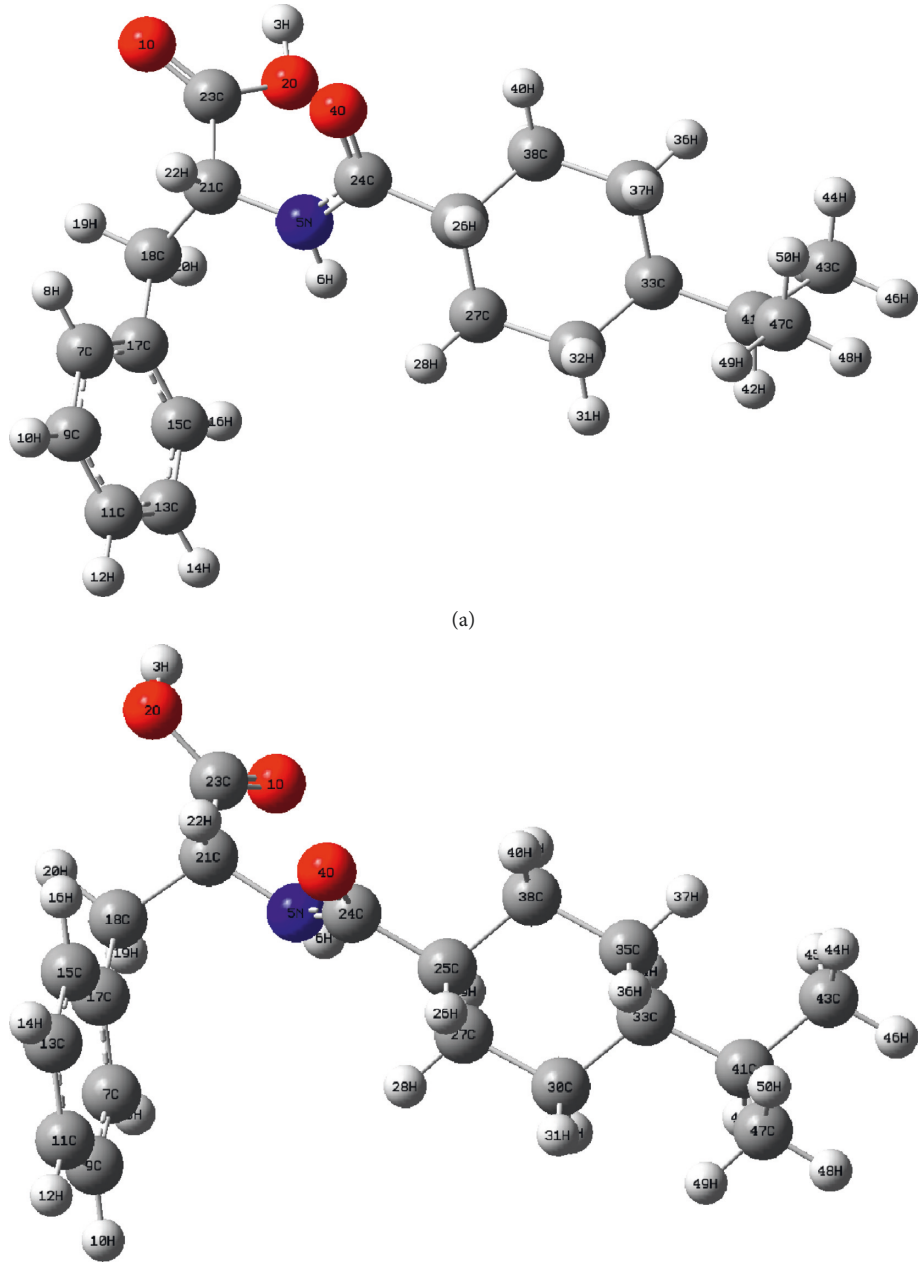

FIGURE 1: The optimized monomer structures of antidiabetic molecule nateglinide: (a) Monomer 1; (b) Monomer 2. Monomer 1: 6-31 + G(d, p); E(RB3LYP) = −1020.83682668 a.u.; dipole moment = 5.1216 debye; Monomer 2: 6–31 + G(d, p); E(RB3LYP) = −1020.83864468 a.u.; dipole moment = 2.3479 debye.

DFT/B3LYP/6-31G + (d, p) level. Scaling factors were used for theoretical vibrational wavenumbers. The computed vibrational wavenumbers were scaled as 0.964 for frequencies at the B3LYP/6-31G + (d, p) basis set [29]. The experimental and simulated IR and Raman spectra of the title compound are given in Figures 2 and 3, respectively.

The characteristic bond of nateglinide was observed at 1647 cm^{-1} with–C=O functional group, 1715 cm^{-1} with –COOH functional group, 2859–3064 cm^{-1} with –CH2 functional group, and 3308 cm^{-1} with –NH functional group [30]. The C=O peak was observed at 1650 cm^{-1} with an intensity of 333.887 D (10–40 $esu^2 \cdot cm^2$) [31]. The C=O stretching vibration of nateglinide was observed at 1711 (IR), 1647 (IR)–1647 (R) cm^{-1}, and 1339 (IR)–1339 (R), and the computed scaled wavenumber values for this band were obtained at 1746 cm^{-1}, 1671 cm^{-1}, and 1341 cm^{-1}.

NH stretching peaks appear at 3585.48 cm^{-1} and 3710.51 cm^{-1} [31]. In the present case, NH stretching modes are calculated at 3508 cm^{-1}.

The peaks at 2921.26 cm^{-1}–3147.88 cm^{-1} range have the highest intensity of 122.03 D (10^{-40} $esu^2 \cdot cm^2$) due to C-H (aromatic) single stretching and OH sharp peak for the

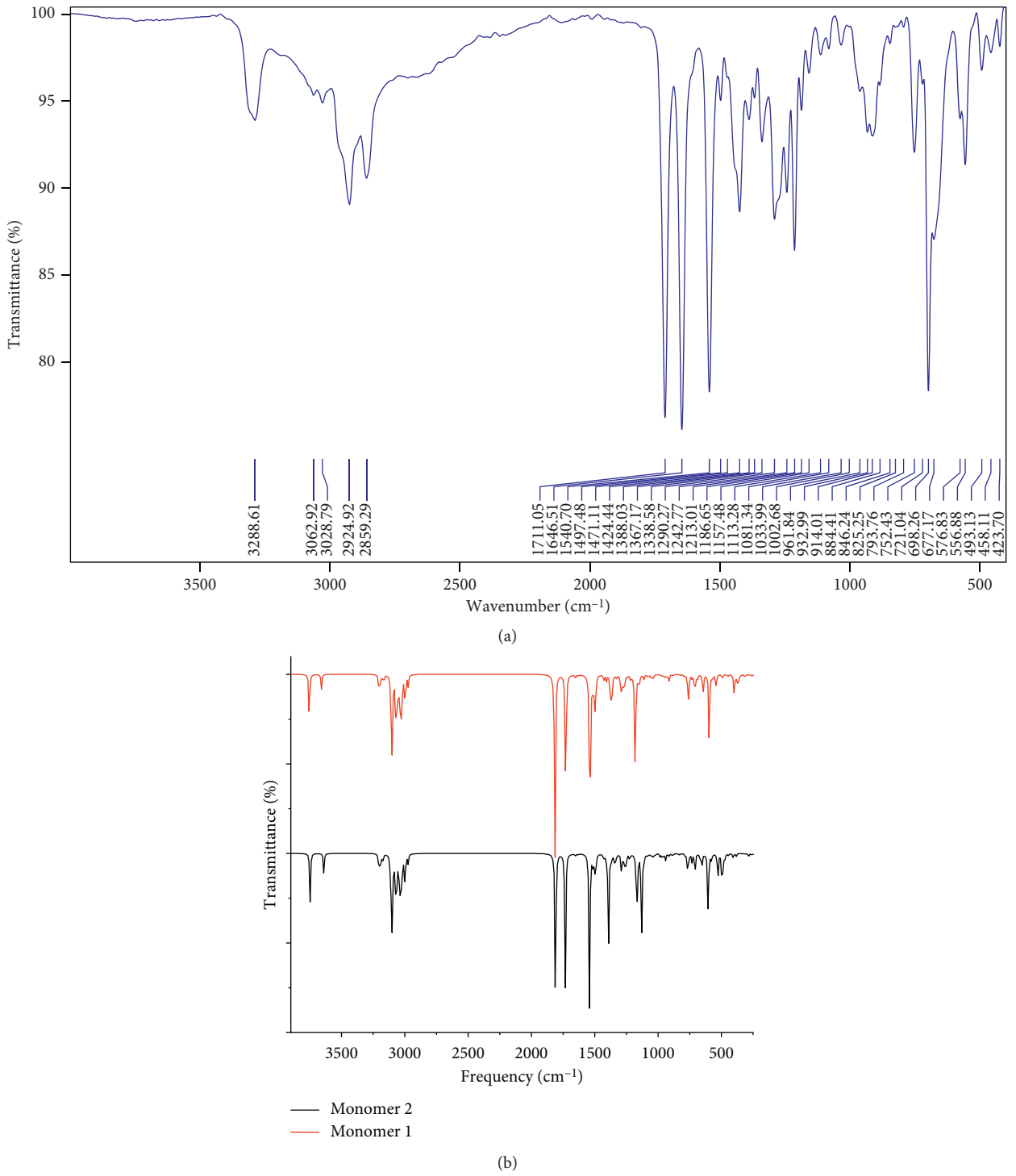

FIGURE 2: The experimental IR spectrum of nateglinide (a) and simulated IR spectra of nateglinide for Monomer 1 and for Monomer 2 (b).

infrared spectrum. There is strong symmetric stretching between carbon and hydrogen (νCH) at 2800–3000 cm^{-1} frequency range for the Raman spectrum [31]. The C-H aromatic stretching vibration and C-H aliphatic stretching vibrations are at 3074 cm^{-1}, 2933 cm^{-1}, and 2860.88 cm^{-1} [32]. The C-H stretching bands in molecule were observed at 3289, 3063 cm^{-1}, 3029 cm^{-1}, 2925 cm^{-1}, and 2859 cm^{-1} in the FT-IR spectrum and at 3285 cm^{-1}, 3063 cm^{-1}, 2937 cm^{-1}, and 2860 cm^{-1} in the Laser-Raman spectrum. These bands were computed at 3091 cm^{-1}, 3079.98 cm^{-1}, 3071 cm^{-1}, 3062 cm^{-1}, 3057 cm^{-1}, 2934 cm^{-1}, 2922 cm^{-1}, and 2868 cm^{-1} in our calculations.

The O-H stretching band in the title molecule was computed at 3613 cm^{-1} in the FT-IR spectrum. The OH in-plane bending vibrations (δHOC) were experimentally obtained at 1290 cm^{-1} (IR) (cal. with 15% contribution of

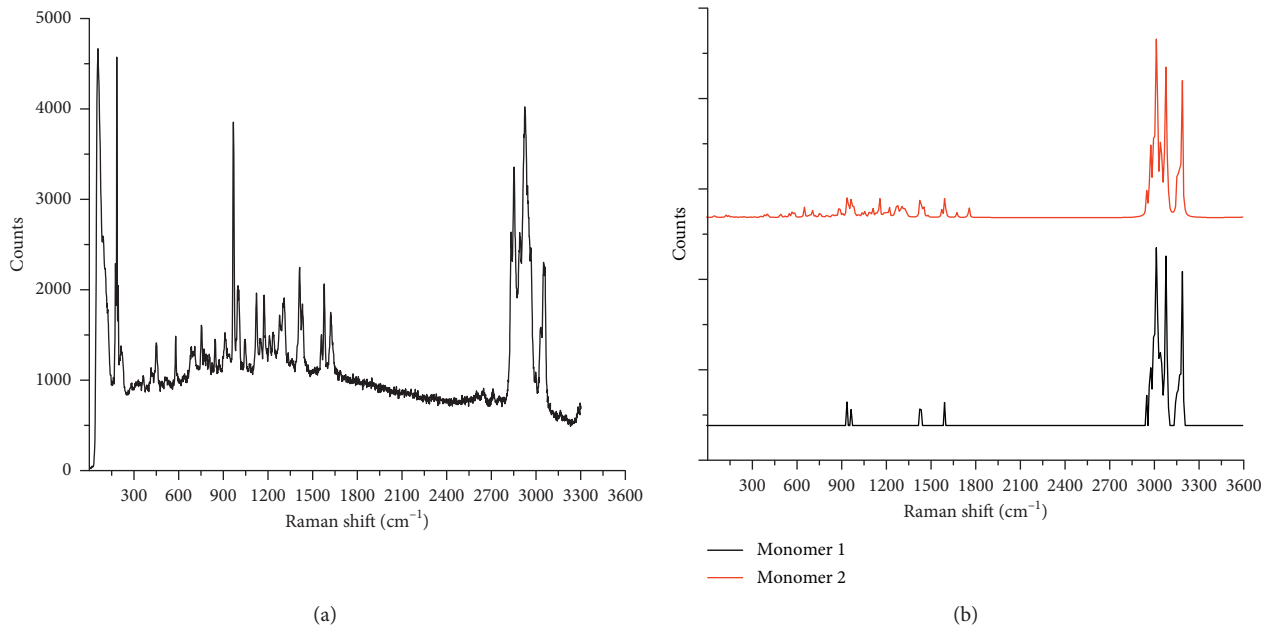

Figure 3: The experimental Laser-Raman spectrum of nateglinide (a) and simulated Raman spectra of nateglinide for Monomer 1 and for Monomer 2 (b).

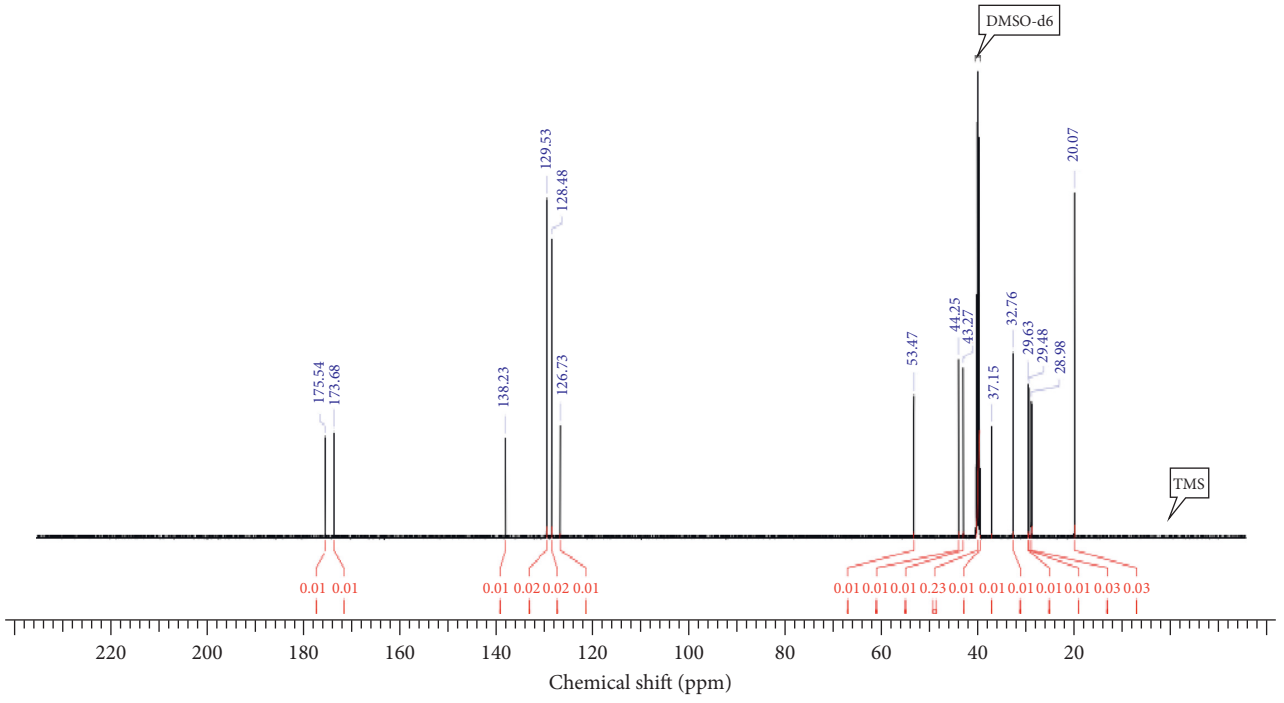

Figure 4: The experimental ^{13}C NMR chemical shift spectra of nateglinide.

PED) and 1243(IR)–1243(R) (cal. with 13% contribution of PED) cm^{-1}. The OH in-plane bending vibrations (δHOC) were calculated at 1291 cm^{-1} (IR) and 1230 cm^{-1} (IR). The OH out-of-plane bending mode (τHOCC) was observed at 1290 cm^{-1} (IR) and 1187 cm^{-1} (IR)–1182 cm^{-1} (R), whereas it was computed at 1291 cm^{-1} and 1180 cm^{-1} with 17% and 13% contribution of PED, respectively.

3.3. ^{1}H and ^{13}C NMR Chemical Shift Analyses. The experimental shielding ranges for ^{1}H NMR and ^{13}C NMR are given as 0–13 ppm and 0–180 ppm, respectively. ^{1}H and ^{13}C NMR chemical shift calculated with gauge-including atomic orbital (GIAO) approach using Gaussian 09 software shows good agreement with the experimental chemical shift. Figures 4 and 5 show the experimental ^{1}H and ^{13}C NMR

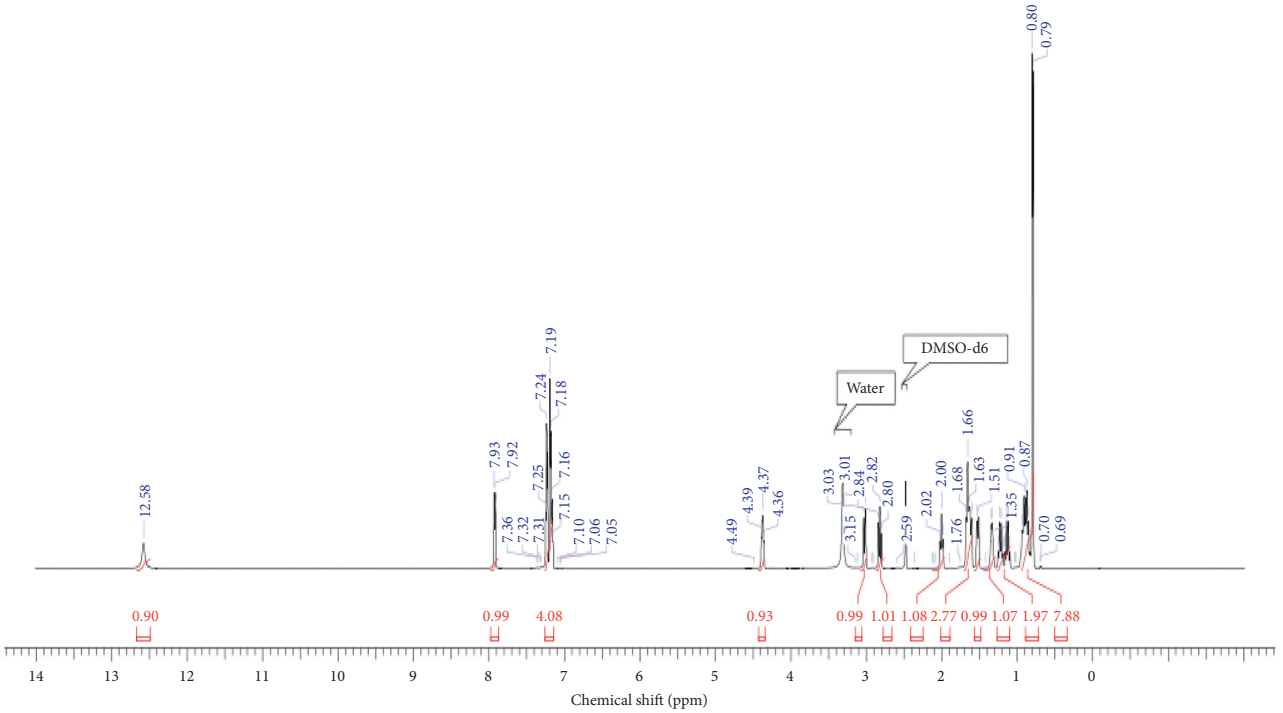

Figure 5: The experimental ^{1}H NMR chemical shift spectra of nateglinide.

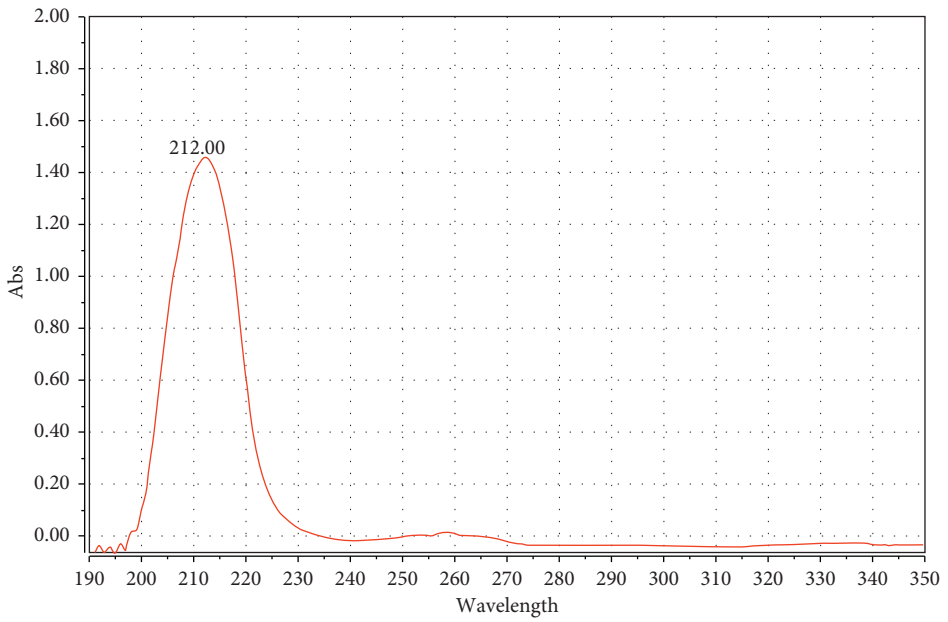

Figure 6: The experimental UV-Vis analysis of antidiabetic molecule nateglinide in methanol.

chemical shift spectra of nateglinide. The experimental ^{1}H and ^{13}C chemical shift values measured in DMSO-d_6 solvent and the chemical shift values calculated at the DFT/B3LYP/6-31G + (d, p) level in DMSO solvent are shown in Tables 5 and 6.

^{1}H chemical shift values for Monomer 1 were computed at the intervals of 0.8078–8.1579 ppm in DMSO. ^{1}H chemical shift values for Monomer 2 were computed at the intervals of 0.8144–8.089 ppm in DMSO. The experimental chemical shifts of ^{1}H are measured in the range of 0.69–12.58 ppm. The largest deviation between the calculated and experimental ^{1}H NMR chemical shifts (δ_{exp}–$\delta_{cal.}$) was obtained for H16 with 0.6135 ppm, whereas the smallest deviation was found for H37 with 0.0009 ppm for Monomer 1. The largest deviation between the calculated and experimental ^{1}H NMR chemical shifts (δ_{exp}–$\delta_{cal.}$) was obtained for H22 with 1.4 ppm, whereas the smallest deviation was found for H34 with 0.0028 ppm for Monomer 2.

Table 1: The experimental and computed vibrational wavenumbers and vibrational assignments of nateglinide results.

Assignment (PED%) Molecular formula: $C_{19}H_{27}NO_3$	Exp. freq. (cm^{-1})		The computed parameters for Monomer 2			
	IR	Raman	Freq.	Scaled freq.	I_{IR}	S_{Raman}
$\nu sO_2H_3(100)$			3748	3613	78.26	226.52
$\nu_s N_5H_6(100)$			3639	3508	32.33	56.46
$\nu sC_9H_{10}(17) + \nu sC_{11}H_{12}(44+ \nu sC_{13}H_{14}(32)$	3289	3285	3206	3091	15.57	292.02
$\nu sC_{13}H_{14}(39) + \nu sC_{15}H_{16}(10)$			3195	3079,98	29.04	42.71
$\nu sC_{15}H_{16}(18)$			3186	3071	8.57	107.31
$\nu sC_{13}H_{14}(22) + \nu sC_{15}H_{16}(67)$	3063	3063	3176	3062	3.57	57.71
$\nu sC_7H_8(68) + \nu sC_9H_{10}(23)$	3029		3171	3057	7.64	33.74
$\nu sC_{18}H_{19}(64) + \nu sC_{18}H_{20}(35)$		2937	3044	2934	22.81	112.46
$\nu sC_{43}H_{44}(28) + \nu sC_{43}H_{45}(32) + \nu sC_{43}H_{46}(28)$	2925		3031	2922	36.09	53.34
$\nu sC_{33}H_{34}(93)$	2859	2860	2975	2868	16.76	44.91
$\nu sO_1C_{23}(86)$	1711		1811	1746	279.97	16.72
$\nu sO_4C_{24}(83)$	1647	1647	1733	1671	224.63	6.75
$\nu sC_9C_7(12) + \nu sC_{15}C_{13}(26)$		1607	1654	1594	4.06	36.96
$\nu sC_{11}C_9(29) + \nu sC_{17}C_7(22) + \delta C_{15}C_{13}C_{11}(12)$	1541		1633	1574	1.19	8.95
$\nu sN_5C_{24}(19) + \delta H_6N_5C_{24}(50)$	1497		1542	1486	257.57	2.00
$\delta H_8C_7C_9(15) + \delta H_{10}C_9C_{11}(18) + \delta H_{14}C_{13}C_{11}(18) + \delta H_{16}C_{15}C_{17}(16) + \delta C_{13}C_{11}C_9(10)$	1471		1534	1479	10.80	0.38
$\delta H_{44}C_{43}H_{46}(20) + \delta H_{46}C_{43}H_{45}(15) + \delta H_{48}C_{47}H_{50}(20) + \delta H_{49}C_{47}H_{48}(24)$		1462	1513	1459	8.37	10.34
$\delta H_{32}C_{30}H_{31}$ (29) + $\delta H_{37}C_{35}H_{36}$ (31)		1440	1490	1436	0.69	8.01
$\delta H_{12}C_{11}C_9$ (18) + $\delta H_{20}C_{18}H_{19}$ (25)	1424		1487	1433	7.34	4.42
$\delta H_{44}C_{43}H_{46}(13) + \delta H_{45}C_{43}H_{44}(10) + \delta H_{48}C_{47}H_{50}(17) + \delta H_{49}C_{47}H_{48}(15) + \delta H_{50}C_{47}H_{49}(15)$	1388		1430	1379	9.88	0.76
$\delta H_{34}C_{33}H_{35}(11) + \delta H_{45}C_{43}H_{44}(11) + \delta H_{46}C_{43}H_{45}(13)$	1367		1411	1360	8.04	0.36
$\nu sO_2C_{23}(12) + \nu sO_{23}C_{21}(10) + \delta H_{22}C_{21}C_{23}(23)$	1339	1339	1391	1341	138.92	6.34
$\nu sC_9C_7(11) + \nu sC_{13}C_{11}(13) + \nu sC_{15}C_{13}(12)+ \delta H_8C_7C_9(16) + \delta H_{12}C_{11}C_9(10) + \delta H_{16}C_{15}C_{17}(19)$		1311	1361	1312	1.08	2.19
$\delta H_3O_2C_{23}(15) + \tau H_{20}C_{18}C_{17}C_{15}(24) + \tau H_{22}C_{21}C_{23}O_2(17)$	1290		1339	1291	12.17	6.90
$\delta H_{26}C_{25}C_{38}(23)$		1268	1314	1267	2.01	1.47
$\delta H_3O_2C_{23}(13) + \delta H_{22}C_{21}C_{23}(28)$	1243	1243	1276	1230	11.37	6.35
$\delta H_{22}C_{21}C_{23}(10)$	1213	1210	1260	1215	35.96	7.82
$\delta H_6N_5C_{24}(11) + \delta H_{19}C_{18}C_{17}(17) + \tau H_{22}C_{21}C_{23}O_2(13)$	1187	1182	1224	1180	10.33	12.41
$\nu sC_{15}C_{13}(11) + \delta H_8C_7C_9(17) + \delta H_{10}C_9C_{11}(16) + \delta H_{14}C_{13}C_{11}(21) + \delta H_{16}C_{15}C_{17}(17)+$	1157	1155	1207	1164	0.71	3.24
$\nu sO_2C_{23}(18) + \nu sN_5C_{21}(35)$	1113		1131	1090	150.02	7.17
$\nu sC_9C_7(19) + \nu sC_{15}C_{13}(16) + \delta H_8C_7C_9(10) + \delta H_{12}C_{11}C_9(12)$	1081	1080	1110	1070	6.74	4.44
$\nu sC_{27}C_{25}(15) + \nu sC_{30}C_{27}(11) + \nu sC_{38}C_{35}(11)$	1034	1037	1089	1050	1.62	3.31
$\nu sC_{38}C_{35}(20)$	1003	1003	1038	1001	2.60	14.97
$\tau H_{10}C_9C_{11}C_{13}(16) + \tau H_{12}C_{11}C_9C_7(31) + \tau H_{14}C_{13}C_{11}C_9(26) + \tau H_{16}C_{15}C_{17}C_{18}(10)$	962		1001	965	0.10	0.23
$\tau H_8C_7C_9C_{11}(14) + \tau H_{10}C_9C_{11}C_{13}(25) + \tau H_{14}C_{13}C_{11}C_9(18) + \tau H_{16}C_{15}C_{17}C_{18}(18)$		948	981	946	0.53	0.73
$\nu sC_{47}C_{41}(10) + \tau H_{49}C_{47}C_{41}C_{33}(10)$	933		966	931	4.13	6.27
$\tau H_{16}C_{15}C_{17}C_{18}(10)$	914	911	942	908	14.03	1.89
$\tau H_8C_7C_9C_{11}(11) + \tau H_{12}C_{11}C_9C_7(13) + \tau H_{16}C_{15}C_{17}C_{18}(10)$	884	880	918	885	0.46	3.67
$\tau H_8C_7C_9C_{11}(26) + \tau H_{10}C_9C_{11}C_{13}(23) + \tau H_{14}C_{13}C_{11}C_9(24) + \tau H_{16}C_{15}C_{17}C_{18}(26)$	825		856	825	0.33	0.73
$\delta C_{13}C_{11}C_9(23)$	794	790	831	801	1.83	3.28
$\tau C_{17}C_7C_9C_{11}(10)$	752	754	766	738	34.94	2.67
$\tau O_4C_{25}N_5C_{24}(25) + \tau O_1C_{21}O_2C_{23}(10)$	721	720	757	730	9.88	1.25
$\nu sC_{21}C_{18}(10) + \delta C_{13}C_{11}C_9(10) + \tau O_1C_{21}O_2C_{23}(36)$	698		733	707	13.36	10.82
$\tau H_8C_7C_9C_{11}(13) + \tau C_{13}C_{11}C_9C_7(13) + \tau C_{15}C_{13}C_{11}C_9(19) + \tau C_{17}C_7C_9C_{11}(22)$	677		709	683	39.63	0.27
$\delta O_1C_{23}O_2(41)$	577	625	655	631	29.30	8.83
$\delta C_{17}C_7C_9(11)$	557		580	559	8.75	2.77
$\gamma C_{41}C_{30}C_{35}C_{33}(12)$	458	458	472	455	7.50	2.39

Table 1: Continued.

Assignment (PED%) Molecular formula: $C_{19}H_{27}NO_3$	Exp. freq. (cm^{-1})		The computed parameters for Monomer 2			
	IR	Raman	Freq.	Scaled freq.	I_{IR}	S_{Raman}
$\boldsymbol{\delta}N_5C_{21}C_{18}(10)$	424		444	428	2.74	0.98
$\boldsymbol{\tau}H_8C_7C_9C_{11}(12) + \boldsymbol{\tau}C_{13}C_{11}C_9C_7(19) + \boldsymbol{\tau}C_{15}C_{13}C_{11}C_9(36)$		406	414	399	0.11	0.03
$\boldsymbol{\delta}O_2C_{23}C_{21}(14)$		261	286	276	5.95	0.70
$\boldsymbol{\tau}C_{38}C_{35}C_{33}C_{30}(12)$		227	241	232	1.00	0.31

s, symmetric; as, asymmetric; **ν**, stretching; **δ**, in-plane bending; **τ**, torsion; **γ**, out-of-plane bending; d_s, scissoring and symmetric bending; **ρ**, rocking; *t*, twisting; *w*, wagging; I_{IR}, IR intensity (km/mol); S_{Raman}, Raman scattering activity; PED, potential energy distribution; *W*, wavenumber (cm^{-1}); *T*, transmittance (%). R^2=0.9981 for Monomer 1 and R^2=0.9980 for Monomer 2 for IR wavenumbers.

Table 2: The experimental and computed UV-Vis parameters and electronic transitions in methanol of nateglinide.

The experimental parameters	Calculated parameter for Monomer 2	The calculated parameters for Monomer 1 (td = (nstates = 6) B3LYP/6–31 + G(d, p) scrf = (cpcm,solvent = methanol) maxdis k = 22 GB geom = connectivity)				
λ_{exp} (nm)	Transitions	λ_{cal} (nm)	λ_{cal} (nm)	Excitation energy (eV)	Oscillator strength	Major contributions [31]
	$n \longrightarrow \sigma^*$	236.49	236.51	5.2421	0.0046	H-1->LUMO (35%), HOMO->L + 1 (41%) H-2->LUMO (3%), H-1->L + 1 (4%), H-1->L + 2 (5%), HOMO->LUMO (9%)
	$n \longrightarrow \sigma^*$	228.64	228.14	5.4345	0.0144	H-3->LUMO (50%), H-3->L + 2 (18%) H-7->LUMO (2%), H-7->L + 2 (2%), H-6->LUMO (3%), H-6->L + 2 (3%), H-1->LUMO (4%), HOMO->LUMO (7%)
	$n \longrightarrow \sigma^*$	219.7	221.79	5.5902	0.0065	H-2->L + 2 (25%), H-2->L + 4 (39%) H-2->LUMO (3%), H-2->L + 3 (5%), H-2->L + 5 (6%), H-1->L + 2 (4%), H-1->L + 4 (5%)
	$n \longrightarrow \sigma^*$	216.37	219.16	5.6571	0.0741	HOMO->LUMO (66%) H-3->LUMO (6%), H-2->LUMO (6%), H-2->L+ 4 (2%), H-1->L + 1 (5%), HOMO->L+ 1 (6%), HOMO->L + 2 (3%)
212	$n \longrightarrow \sigma^*$	212.63	216.85	5.7175	0.0120	H-2->LUMO (67%), H-1->LUMO (12%) H-3->LUMO (6%), H-2->L + 4 (5%), HOMO->LUMO (2%)
	$n \longrightarrow \sigma^*$	210.78	207.28	5.9814	0.0257	H-1->LUMO (13%), H-1->L + 1 (18%), HOMO->L + 2 (50%) H-2->LUMO (4%), H-1->L + 2 (6%)

The ^{13}C chemical shifts for Monomer 1 were calculated in the range of 7.0408–163.551 ppm in DMSO ppm, and the ^{13}C chemical shifts for Monomer 2 were calculated in the range of 6.1516–161.592 ppm, while they were experimentally recorded in the range of 20.07–175.54 ppm. The largest deviation between the calculated and experimental ^{13}C NMR chemical shifts (d_{exp}–$d_{cal.}$) was obtained for C17 with 14.022 ppm, whereas the smallest deviation was found for C33 with 0.6225 ppm for Monomer 1. The largest deviation between the calculated and experimental ^{13}C NMR chemical shifts (d_{exp}–$d_{cal.}$) was obtained for C23 with 13.948 ppm, whereas the smallest deviation was found for C33 with 0.4279 ppm for Monomer 2.

3.4. UV-Vis Analyses. The obtained and simulated UV-Vis spectrum of nateglinide dissolved in methanol was recorded in the region of 190–350 nm. UV-Vis calculation was performed in methanol using the TD-DFT method with Gaussian 09W software and GaussView5 molecular visualization program. The measured and simulated UV-Vis electronic absorption spectra are given in Figures 6 and 7. Additionally, the experimental and computed electronic absorption wavelengths, electronic transitions, oscillator strengths, excitation energies, and major contributions are listed Table 2. Rajasekaran et al. determined a method in which the absorbance of pure drug and tablet extract in 95% ethanol was measured at 210 nm [33]. Xavier studied the UV

Table 3: The optimized molecular geometric parameters of nateglinide.

Bond lengths (Å)	X-ray [27]	Values	Bond lengths (Å)	X-ray [27]	Values	Bond angles (°)	Values	X-ray [27]	Bond angles (°)	Values	X-ray [27]
C11-C13	1.352	1.398	C24-C25	1.495	1.530	C11-C13-H14	120.102	119.116	C25-C38-C35	111.408	110.700
C13-C15	1.413	1.395	C25-C38	1.537	1.546	C15-C13-H14	119.705	119.160	C38-C35-C33	112.186	112.617
C9-C11	1.360	1.396	C35-C38	1.524	1.537	C9-C11-H12	120.254	120.606	C35-C33-C30	109.752	110.312
C7-C9	1.404	1.398	C33-C35	1.527	1.542	C13-C11-H12	120.199	120.467	C33-C30-C27	112.163	112.776
C7-C17	1.374	1.401	C33-C30	1.522	1.542	C13-C15-H16	119.437	120.306	H28-C27-H29	107.285	108.188
C15-C17	1.392	1.403	C27-C30	1.527	1.539	C11-C9-H10	120.189	119.550	C27-C25-H26	108.092	106.800
C17-C18	1.524	1.514	C25-C27	1.532	1.539	C17-C15-H16	119.745	120.288	H39-C38-H40	107.036	108.165
C18-C21	1.526	1.558	C33-C41	1.542	1.554	C7-C9-H10	119.774	119.650	C35-C33-H34	106.915	106.334
C21-C23	1.522	1.525	C41-C47	1.493	1.539	C17-C7-H8	119.457	119.513	H37-C35-H36	106.559	107.896
C23=O1	1.231	1.213	C41-C43	1.543	1.539	C17-C18-H20	110.141	108.536	H31-C30-H32	106.523	107.730
C23=O2	1.308	1.353	C24=O4	1.252	1.230	C17-C18-H19	109.619	108.510	C33-C41-H42	105.779	106.849
O2-H3	0.909	0.973	N5-H6	0.927	1.010	C21-C18-H19	108.662	108.488	H44-C43-H45	107.793	109.495
C21-N5	1.460	1.447	C24=N5	1.332	1.372	C21-C18-H20	107.531	108.534	C41-C43-H46	110.750	109.459
Dihedral angles (°)						C23-C21-H22	108.860	107.886	H42-C41-C47	107.149	106.767
H10-C9-C7-C17		179.820		179.844		N5-C21-H22	106.696	107.947	C41-C47-H50	111.618	109.518
H10-C9-C11-C13		−179.816		178.624		C24-N5-H6	119.107	121.393	H49-C47-H48	107.337	109.401
H16-C15-C13-C11		−179.772		178.229		C23-O2-H3	107.493	106.777	C25-C24-O4	120.642	121.732
C9-C7-C17-C18		−179.489		−179.882		O4-C24-N5	121.982	119.602	C24-C25-C27	117.171	116.594
C21-C23-O2-H3		−177.502		178.064		O1-C23-O2	122.883	124.478	C24-C25-C38	109.582	109.451
C21-N5-C24-C25		−174.757		−170.842		N5-C24-C25	117.375	118.654	C25-C27-C30	110.933	109.665
C25-C38-C35-H36		−65.703		−65.679							

[27] L. Tessler, I. Goldberg., bis(nateglinide) hydronium chloride, and its unique self-assembly into extended polymeric arrays via O-H···O, N-H···Cl, and O-H···Cl hydrogen bonds. Acta Cryst. C61 (2005) 738–740.

Table 4: Zero point, relative energy and dipole moment of nateglinide.

Conformers	Zero-point energy (Hartree/particle)	Relative energy (kcal/mole)	Dipole moment (debye)
Monomer 1	−1020.402782	0.99582	5.1216
Monomer 2	−1020.404370		2.3479

Table 5: The experimental and computed ^{1}H NMR isotropic chemical shifts (with respect to TMS, all values in ppm) of nateglinide.

δ_{exp} (in DMSO-d_6)	Monomer 1 δ_{cal} (in DMSO)	Monomer 2 δ_{cal} (in DMSO)	δ_{exp} (in DMSO-d_6)	Manomer 1 δ_{cal} (in DMSO)	Manomer 2 δ_{cal} (in DMSO)
12.58			1.76	1.78-H42	1.88-H37
	8.16-H8	8.09-H16	1.68	1.67-H31	1.83-H26
	8.07-H10	7.89-H10	1.66	1.67-H28	1.65-H32
7.93–7.92	7.95-H14	7.84-H14	1.63	1.61-H34	1.55-H29
7.24–7.36	7.83-H12	7.78-H12	1.51	1.54-H29	1.51-H34
7.15–7.19	7.80-H16	7.70-H8		1.50-H32	1.50-H31
7.05–7.10	6.92-H3	7.10-H3		1.49-H39	1.31-H39
	6.16-H6	6.20-H6	1.35	1.35-H37	1.23-H44
4.36–4.49	4.55-H22	5.76-H22		1.25-H44	1.23-H36
3.01–3.15	3.48-H19	3.71-H20		1.19-H46	1.21-H49
2.80–2.84	2.93-H20	2.67-H19		1.13-H49	1.19-H46
2.59	2.17-H26	2.05-H40		1.10-H45	1.08-H45
2.00–2.02	2.15-H40	1.94-H42	0.91, 0.87	0.86-H48	0.96-H48
	1.97-H36	1.88-H28	0.69, 0.70	0.81-H50	0.81-H50

R^2 = 0.9932 and RMSD = 0.237831578 ppm for Monomer 1 and R^2 = 0.9709 and RMSD = 0.403748 ppm for Monomer 2.

detector response of NTG and found the best result at 210 nm [19]. In this research, the wavelength recorded at 212 nm in the experimental UV-Vis spectrum can be assigned to $n \longrightarrow \sigma*$ transition. The calculated wavelength corresponding to this experimental value was obtained at 216.85 nm with 5.7175 eV value of excitation energy and 0.0120 value of oscillator strength for Monomer 1. The other computed wavelengths are given as 236.51 nm, 228.14 nm, 221.79 nm, 219.16 nm, 216.85 nm, and 207.28 nm. The experimental and computed wavelengths and electronic transitions are in good harmony. The calculated wavelength corresponding to this experimental value was obtained at

Table 6: The experimental and computed ^{13}C NMR isotropic chemical shifts (with respect to TMS, all values in ppm) of nateglinide.

δ_{exp} (in DMSO-d_6)	Monomer 1 δ_{cal} (in DMSO)	Monomer 2 δ_{cal} (in DMSO)	δ_{exp} (in DMSO-d_6)	δ_{cal} (in DMSO)	Monomer 2 δ_{cal} (in DMSO)
175.54	163.551-C24	161.592-C23	43.27, 44.25	39.6492-C25	39.5256-C25
173.68	161.646-C23	161.179-C24	37.15	36.5275-C33	36.7221-C33
138.23	124.208-C17	124.354-C17	32.76	30.134-C18	33.2255-C18
129.53	115.937-C9	116.639-C7	29.63	27.5208-C41	27.5424-C41
128.48	115.795-C15	115.406-C15	29.48	25.2552-C38	25.943-C38
126.73	115.334-C13	114.909-C9	28.98	24.9742-C30	24.3689-C30
	114.87-C7	114.799-C13	20.07	21.5326-C27	21.083-C27
	113.289-C11	112.649-C11		18.302-C35	17.7894-C35
53.47	50.3871-C21	44.1719-C21		12.926-C43	13.0837-C43
				7.0408-C47	6.1516-C47

$R^2 = 0.9985$ and RMSD = 8.615417071 ppm for Monomer 1 and $R^2 = 0.9981$ and RMSD = 9.136034 ppm for Monomer 2.

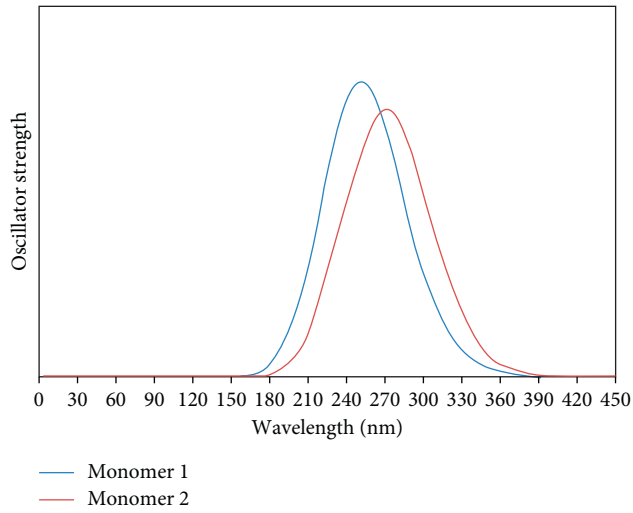

Figure 7: The simulated UV-Vis analysis of nateglinide in methanol, Monomer 1 and Monomer 2.

212.63 nm with 5.8310 eV value of excitation energy and 0.0133 value of oscillator strength for Monomer 2. The other computed wavelengths are given as 228.64 nm, 219.70 nm, 216.37 nm, 212.63 nm, and 210.78 nm.

3.5. HOMO-LUMO Analyses. The computed molecular energies for Monomer I and Monomer II were obtained as $E = -1020.83682668$ a.u. and $E = -1020.83864468$ a.u., respectively. The calculated dipole moments are 5.1216 and 2.3479 debye for Monomer I and Monomer II, respectively. By considering Monomer II, the structural, spectroscopic (IR, Raman, NMR, and UV-Vis), and HOMO-LUMO analyses for nateglinide were performed using theoretical computational methods. The relative energy between the two monomers is considerably low, and it has a value of −0.99582 kcal/mole. Owing to its more stable structure, dipole moment of monomer 2 is lower than monomer 1. The simulated HOMO and LUMO surfaces, energy values, and their shapes for the title molecule are given in Figure 8. The calculated HOMO and LUMO energy values were computed as −6.9449 eV and −0.8923 eV for Monomer 1 and −6.8336 eV and −0.8101 eV for Monomer 2 at the DFT/B3LYP/6-31G + (d, p) level, respectively.

4. Conclusion

The structural, spectroscopic (IR, Laser-Raman, NMR, and UV-Vis), and HOMO-LUMO analyses for nateglinide were performed using theoretical computational methods. The computed spectral properties were compared with the experimental data. After the conformational analysis, two molecular geometric forms at the lowest energies were optimized with the DFT/B3LYP/6-31G + (d, p) level. The results can be summarized as follows:

(i) The linear correlation coefficient (R^2) value between the calculated and experimental [27] molecular geometric parameters was found as 0.975 for bond lengths (Å) and 0.9605 for bond angles (°), respectively, as given in Table 3.

(ii) As a result of the performed analyses, the linear correlation coefficient (R^2) values between the experimental and computed vibrational frequencies of Monomer 1 and Monomer 2 for IR wavenumbers were found as $R^2 = 0.9981$ and $R^2 = 0.9980$, respectively.

(iii) The R^2 and RMSD values between the experimental and computed ^1H NMR chemical shifts were found

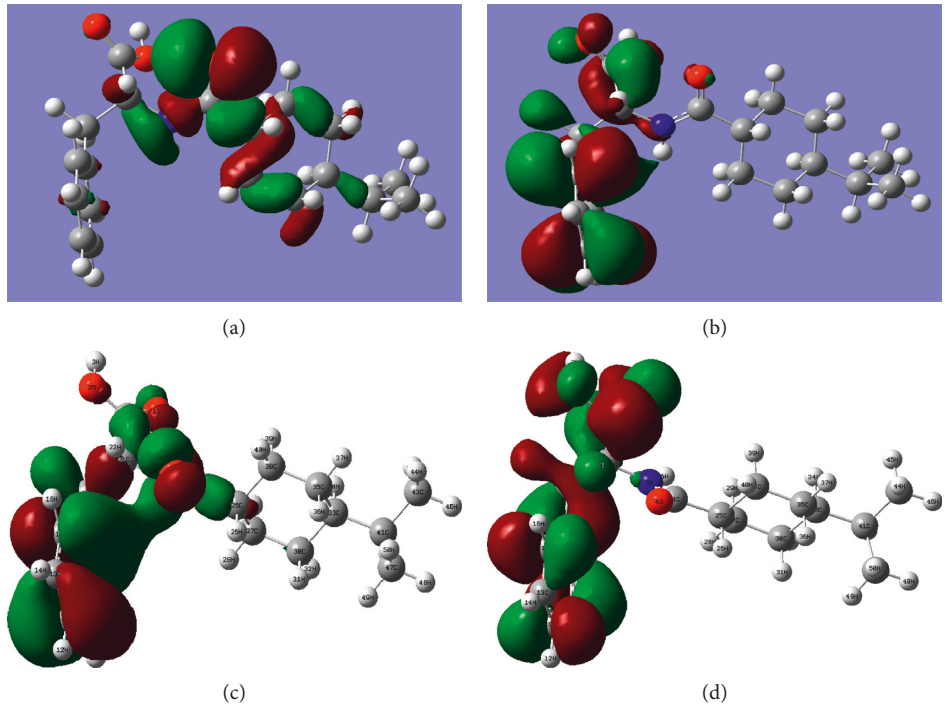

(a) (b) (c) (d)

Figure 8: The HOMO and LUMO energy plots of nateglinide molecule. (a) Monomer 1: HOMO = −6.9449 eV. (b) Monomer 1: LUMO = −0.8923 eV. (c) Monomer 2: HOMO = −6.8336 eV. (d) Monomer 2: LUMO = −0.8101 eV.

as 0.9932 and 0.24 ppm for Monomer 1 and as 0.9709 and 0.40 ppm for Monomer 2, respectively. The R^2 and RMSD values between the experimental and computed ^{13}C NMR chemical shifts were found as 0.9985 and 8.62 ppm for Monomer 1 and as 0.9981 and 9.14 ppm for Monomer 2, respectively.

(iv) The major contributions for Monomer 1 were found as H-2->LUMO (67%), H-1->LUMO (12%) H-3->LUMO (6%), H-2->L + 4 (5%), and HOMO->LUMO (2%) for 216.85 nm wavelength. The major contributions for Monomer 2 were found as H-3->LUMO (64%), H-1->LUMO (10%) H-1->L + 2 (6%), HOMO->LUMO (3%), and HOMO->L + 1 (4%) for 212.63 nm wavelength.

Data Availability

The data used to support the findings of this study are available from the corresponding author upon request.

Additional Points

(i) The optimized molecular geometry and molecular parameters of nateglinide molecule were investigated. (ii) Molecular structure of nateglinide molecule was studied using DFT. (iii) The complete assignments were performed on the basis of the PED. (iv) The vibrational wavenumbers (FT-IR and Laser-Raman) and UV-Vis spectroscopy were studied using experimental and theoretical methods. (v) The experimental and computed proton and carbon-13 NMR chemical shifts were determined. (vi) All the results were compared with experimental (FT-IR, FT-Raman, UV-Vis, and NMR) spectra.

Conflicts of Interest

The author declares that there are no conflicts of interest.

Acknowledgments

This work was supported by Bartin University Research Fund Project under the Project no. 2017-FEN-A-005. The author thanks Cankiri Karatekin University Research Center for NMR, FT-IR, and UV-Vis analysis and Niğde Ömer Halisdemir University Center Research Laboratory for Laser-Raman analysis. The valuable help of Assoc. Prof. Dr. Halil Gökçe, Assoc. Prof. Dr. Halil Oturak, Asst. Prof. Adnan Sağlam, Asst. Prof. Firdevs Banu Özdemir, Pharmaceutist Ali Ünsal Keskiner, and Res. Asst. Mecit Öge is also acknowledged.

References

[1] Novartis, Starlix® (nateglinide) tablets, http://www.pharma.us.novartis.com/product/pi/pdf/Starlix.pdf/, 2013.

[2] N. Nordisk, "Prandin® (repaglinide) tablets," July 2018, http://www.novo-pi.com/prandin.pdf/.

[3] J. S. Grant and L. J. Graven, "Progressing from metformin to sulfonylureas or meglitinides," *Workplace Health and Safety*, vol. 64, no. 9, pp. 433–439, 2016.

[4] J. F. McLeod, "Clinical pharmacokinetics of nateglinide," *Clinical Pharmacokinetics*, vol. 43, no. 2, pp. 97–120, 2004.

[5] N. R. Pani, L. K. Nath, S. Acharya, and B. Bhuniya, "Application of DSC, IST, and FTIR study in the compatibility

testing of nateglinide with different pharmaceutical excipients," *Journal of Thermal Analysis and Calorimetry*, vol. 108, no. 1, pp. 219–226, 2012.

[6] R. Landgraf, "Meglitinide analogues in the treatment of type 2 diabetes mellitus," *Drugs & Aging*, vol. 17, no. 5, pp. 411–425, 2000.

[7] R. E. Pratley, J. E. Foley, and B. E. Dunning, "Rapid acting insulinotropic agents: restoration of early insulin secretion as a physiologic approach to improve glucose control," *Current Pharmaceutical Design*, vol. 7, no. 14, pp. 1375–1397, 2001.

[8] https://www.sigmaaldrich.com/catalog/product/usp/1457607?lang=en&region=TR&cm_sp=Insite-_-prodRecCold_xviews-_-prodRecCold10-2, April 2018.

[9] S. Jain, A. Bhandari, and S. Purohit, "Spectrophotometric determination of nateglinide in bulk and tablet dosage forms," *Asian Journal of Pharmaceutics*, vol. 3, no. 3, 2009.

[10] G. R. Babu, A. L. Rao, S. L. Surekha, T. Kalapraveen, and P. S. Rao, "Spectrophotometric methods for estimation of Nateglinide in bulk drug and its dosage form," *International Journal of Pharmaceutical, Chemical And Biological Sciences*, vol. 3, no. 4, pp. 1160–1164, 2013.

[11] G. R. Babu, A. L. Rao, S. L. Surekha, T. Kalapraveen, and P. S. Rao, "Quantitative estimation of nateglinide in pharmaceutical dosage forms by visible spectrophotometry," *IJRPC*, vol. 3, no. 4, pp. 803–807, 2013.

[12] G. Bruni, V. Berbenni, C. Milanese et al., "Determination of the nateglinide polymorphic purity through dsc," *Journal of Pharmaceutical and Biomedical Analysis*, vol. 54, no. 5, pp. 1196–1199, 2011.

[13] R. Guardado-Mendoza, A. Prioletta, L. M. Jiménez-Ceja, A. Sosale, and F. Folli, "State of the art paper the role of nateglinide and repaglinide, derivatives of meglitinide, in the treatment of type 2 diabetes mellitus," *Archives of Medical Science*, vol. 5, pp. 936–943, 2013.

[14] A. P. Rani, C. B. Sekaran, N. Archana, P. S. Teja, and B. Aruna, "Vis-spectrophotometric methods for the determination of nateglinide," *International Journal of Chemical Sciences*, vol. 7, no. 3, pp. 1642–1652, 2009.

[15] P. Goyal, D. Rani, and R. Chadha, "Exploring structural aspects of nateglinide polymorphs using powder x-ray diffraction," *International Journal of Pharmacy and Pharmaceutical Sciences*, vol. 9, no. 10, pp. 119–127, 2017.

[16] M. Remko, "Theoretical study of molecular structure, pKa, lipophilicity, solubility, absorption, and polar surface area of some hypoglycemic agents," *Journal of Molecular Structure: THEOCHEM*, vol. 897, no. 1–3, pp. 73–82, 2009.

[17] M. Karakaya, Y. Sert, M. Kürekçi, B. Eskiyurt, and Ç. Çırak, "Theoretical and experimental investigations on vibrational and structural properties of tolazamide," *Journal of Molecular Structure*, vol. 1095, pp. 87–95, 2015.

[18] T. Özdemir and H. Gökce, "FT-IR, Raman, and NMR spectroscopy and DFT theory of Glimepiride molecule as a Sulfonylurea compound," *Journal of Applied Spectroscopy*, vol. 85, no. 3, pp. 560–572, 2018.

[19] C. M. Xavier, *Analytical studies on some anti-diabetic drugs*, Ph.D. thesis, University of Mysore, Mysore, Karnataka, India, 2015.

[20] A. D. Becke, "Density-functional thermochemistry. III. The role of exact exchange," *Journal of Chemical Physics*, vol. 98, no. 7, pp. 5648–5652, 1993.

[21] C. Lee, W. Yang, and R. G. Parr, "Development of the Colle-Salvetti correlation-energy formula into a functional of the electron density," *Physical Review B*, vol. 37, no. 2, pp. 785–789, 1988.

[22] A. Frish, A. B. Nielsen, and A. J. Holder, *Gauss View User Manual*, Gaussian Inc., Pittsburg, PA, USA, 2001.

[23] M. J. Frisch, G. W. Trucks, H. B. Schlegel et al., *Gaussian 09, Revision, A.1*, Gaussian Inc., Wallingford, CT, USA, 2009.

[24] Gaussian Website, *Visualizing Molecules & Reactions with Gaussview 5*, August 2016, http://www.gaussian.com/g_prod/gv5.htm.

[25] M. H. Jamr'oz, "Vibrational energy distribution analysis VEDA4," *Spectrochimica Acta Part A: Molecular and Biomolecular Spectroscopy*, vol. 114, pp. 220–230, 2004.

[26] M. O'boyle, A. L. Tenderholt, and K. M. Langner, "Cclib: a library for package-independent computational chemistry algorithms," *Journal of Computational Chemistry*, vol. 29, no. 5, pp. 839–845, 2008.

[27] L. Tessler and I. Goldberg, "Bis(nateglinide) hydronium chloride, and its unique self-assembly into extended polymeric arrays via O-H...O, N-H...Cl and O-H...Cl hydrogen bonds," *Acta Crystallographica Section C Crystal Structure Communications*, vol. 61, no. 12, pp. 738–740, 2005.

[28] V. Jain, D. K. Dhaked, Y. Kasetti, and P. V. Bharatam, "Computational study on the conformational preferences in nateglinide," *Journal of Physical Organic Chemistry*, vol. 25, no. 8, pp. 649–657, 2012.

[29] https://cccbdb.nist.gov/vibscalejust.asp, March 2018.

[30] N. Pandey, A. N. Sah, and K. Mahara, "Formulation and evaluation of floating microspheres of nateglinide," *International Journal of Pharma Sciences aand Research*, vol. 7, no. 11, pp. 453–464, 2016.

[31] M. Sa'id, A. S. Bayero, and U. L. Ali, "Determination of infrared, raman, (^{1}H and ^{13}C)-Nmr spectra and density of state of nateglinide oral antidiabetic drug," *International Journal of Nanomedicine and Nanosurgery*, vol. 4, no. 1, 2018.

[32] A. Patil, B. G. Desai, H. N. Shivakumar, and Purvang, "enhancement of nateglinide solubility and dissolution rate," *Research Journal of Pharmacy and Technology*, vol. 4, no. 7, pp. 1159–1164, 2011.

[33] A. Rajasekaran, S. Murugesan, M. K. A. Hathi et al., "Spectrophotometric and chromatographic assay of Nateglinide," *Indian Journal Pharmaceutical Sciences*, vol. 66, p. 806, 2004.